Imaging of Scattering Media by Diffusion Tomography: An Iterative Perturbation Approach

Yao Wang†, Jeng-Hwa Chang and Raphael Aronson*
Departments of Electrical Engineering and Physics*
Polytechnic University, Brooklyn, NY 11201

Randall L. Barbour, Harry L. Graber, and Jack Lubowsky
Departments of Pathology and Biophysics
SUNY Health Science Center, Brooklyn, NY 11203

†Author to whom inquiries should be addressed.

Abstract

This paper describes an iterative perturbation approach for imaging the absorption properties of a dense scattering medium. This method iteratively adjusts a current estimate until the calculated photon fluxes for the estimated medium match the detected readings. The inverse update in each iteration is accomplished by solving a linear perturbation equation. It is similar to the compensation theory method used in electrical impedance tomography. A comparison was made between the methods of conjugate gradient descent and projection onto convex sets for the solution of the perturbation equation. The former converges more rapidly, but can yield an inaccurate solution when the problem is underdetermined. The latter can incorporate many types of *a priori* information to reach a correct solution, but progresses very slowly. A multi-grid, progressive reconstruction technique is proposed, which computes the fine details with the help of the coarse structure. It is quite effective in forcing the correct solution and reducing computation time. These methods have been used to reconstruct several inhomogeneous media containing simple structures, from steady-state reflectance data. Two sets of data are tested: one calculated according to the perturbation model, and the other using Monte-Carlo methods. When the difference between the absorption distributions of the test medium and the initial estimate is localized, a single step of the perturbation approach can resolve the absorption distribution reasonably well to within 5 transport mean free pathlengths from the surface. At greater depths, the reconstruction is less reliable.

1 Introduction

This paper considers the problem of imaging the absorption properties of the interior of a dense scattering medium by analyzing the diffusely scattered field at the surface. It is an extremely difficult problem due to the randomness of the paths traveled by injected particles. Our approach consists of iterative executions of forward and inverse solutions. It iteratively perturbs a current estimate until the calculated photon fluxes for the estimated medium match with the detected. At each iteration, using the previous result as the reference, it produces a new estimate by solving a linear perturbation equation. The coefficients in the equations, to be referred to as *weights*, are the gradients of the detector readings with respect to the absorption properties of the points inside the medium [1, 2]. The idea of weights, or importance functions, is commonly used in the control of nuclear reactors [3]. For isotropically scattering media with steady-state measurements, the weight of a given point for a chosen source–detector pair is the product of the forward and adjoint fluxes at that point. The forward flux is proportional to the collision density at the point for photons injected from the source; the adjoint represents the time-reversed photon path entering the detector, and is proportional to the collision density when photons are launched from the detector. This result is a counterpart of the sensitivity theorem used in electrical impedance tomography (EIT) [4]. The derivation of the detector readings and weights for

0-8194-0787-9/92/$4.00

the current estimated image constitutes the forward problem. The solution of the linear perturbation equation is the inverse problem. The latter is equivalent to the update in the Newton-Raphson minimization method (also known as Gauss-Newton Method) [5]. The general approach is, therefore, similar to the compensation theorem method used in EIT, which combines the sensitivity theorem with the Newton-Raphson update [4].

Until now, we have attempted only one iteration of the perturbation approach using homogeneous media as references. We have calculated forward solutions, i.e, the detector readings and weights for the initial reference medium, using Monte-Carlo methods. For more details on the forward calculation, see Ref. [2] for the steady-state measurement, and Ref. [6] for the time-resolved case. This paper focuses on the solution of the perturbation equation. The problem is difficult, due to the extremely large numbers of the unknowns, the noise characteristics of the measured data, as well as the underdetermined, or ill-posed, nature of the problem. Several iterative reconstruction techniques, have previously been developed, based on the concept of backprojection used in conventional X-ray CT [2]. Here, the *Projection onto Convex Sets* (POCS) and (*Conjugate Gradient Decent*) (CGD) methods have been closely examined and compared. A new multi-grid reconstruction scheme has also been developed. Our focus has been on how to force an algorithm to move towards the correct solution when the problem is underdetermined. Results obtained indicate that even when only steady-state backscattered field is considered, the absorption properties of a scattering medium can be recovered to within 5 transport mean free pathlengths (mfp) from the surface.

2 Reconstruction by Iterative Perturbation

Consider a measuring system where photons are injected with intensities $S_j, j = 1, 2 \ldots, J$, at J source locations on the surface of the test medium, and the photon fluxes $I_{jk}, k = 1, 2, \ldots, K_j$ are measured at K_j detector positions for the j-th incident signal. It is assumed that collimated source and detectors are used, but other configurations can also be considered. The measurement can be either steady-state or time-gated. In addition, the sources and detectors can either be placed around the entire or only portion of the surface of the medium. One special case is when the sources and detectors are placed on one side of the medium and the backscattered field alone is measured. This measuring strategy affords more feasible implementation, but the reconstruction from such measurements is more difficult.

Let the unknown medium be divided into N contiguous non-overlapping small volume elements, or voxels. Let x_i represent the vector containing the unknown parameters at voxel i (a scalar if only one property, say the absorption coefficient, is to be estimated). The goal is to reconstruct the optical properties of all the voxels, $x_i, i = 1, 2, \cdots, N$, from the $M = \sum_{j=1}^{J} K_j$ measurements, $I_{jk}, k = 1, 2, \ldots, K_j; j = 1, 2, \ldots, J$. In this paper, we assume that the scattering property is known, and consider the recovery of the absorption properties. The scalar x_i represents the absorption coefficient in voxel i, which is defined as the ratio of the macroscopic absorption cross-section at this voxel, Σ_{ai}, to the macroscopic total cross-section Σ_{ti}.

For an arbitrary object, the relation between the photon fluxes I_{jk} on the surface and the absorption properties x_i in the interior can be very complicated. A simple approximation to this relation is given by the diffusion equation [7]. However, even with this simplification, closed-form solutions of the forward problem, i.e, determining I_{jk} from the given x_i and S_j, are available only for media having simple and regular geometric structures. The inverse solution, i.e, reconstructing x_i from S_j and I_{jk}, has been considered by many as intractable. In order to overcome difficulties in solving the inverse problem, we have adopted a *perturbation* approach. It assumes that the absorption coefficients of an unknown object, x_i, are very close to those of a reference medium, x_i^r. Suppose the detector readings for the test and reference media are respectively I_{jk} and I_{jk}^r. The perturbation model relates the differences between the absorption properties of the two media ($\Delta x_i = x_i - x_i^r$) with the changes in detector readings ($\Delta I_{jk} = I_{jk}^r - I_{jk}$) by the following first order

approximation:

$$\sum_i w_{ijk}\Delta x_i = \Delta I_{jk}, \quad k = 1, 2, \ldots, K_j,\ j = 1, 2, \ldots, J. \tag{1}$$

Here, $w_{ijk} = -\frac{\partial I^r_{jk}}{\partial x_i}$ is called the *weight*, which specifies the reduction of the photon flux at detector k due to the increase in absorption at voxel i when photons are injected from source j. Let $\mathbf{x}^r$, $\mathbf{x}$, $\mathbf{\Delta x}$ and $\mathbf{w}_{jk}$ represent the vectors composed of, respectively, the elments $x^r_i, x_i, \Delta x_i$ and w_{ijk} for $i = 1, 2, \ldots, N$. Eq. (1) can then be recast as

$$\mathbf{w}^T_{jk}\mathbf{\Delta x} = \Delta I_{jk}, \quad k = 1, 2, \ldots, K_j,\ j = 1, 2, \ldots, J. \tag{2}$$

Let $\mathbf{\Delta I}$ be the vector consisting of ΔI_{jk}, and $\mathbf{W}$ the matrix containing $\mathbf{w}_{jk}$ as row vectors. The above equations can then be written as:

$$\mathbf{W\Delta x} = \mathbf{\Delta I}\,. \tag{3}$$

The vector $\mathbf{w}_{jk}$ will be called the weight vector for the jk-th source–detector pair, and the matrix $\mathbf{W}$ the weight matrix. They are functions of the properties of the reference medium, $\mathbf{x}^r$.

Given $\mathbf{\Delta I}$ and $\mathbf{W}$, $\mathbf{\Delta x}$ can be determined by solving the linear equation (3). Once $\mathbf{\Delta x}$ is found, $\mathbf{x}$ can be readily identified. When the reference medium is very different from the test medium, the approximation in Eqs. (1)–(3) is inaccurate. Hence the above process should be repeated a number of times, with the reference image and the weight matrix being updated after each iteration. The process can be stopped when the difference between two successive estimates becomes smaller than a prescribed threshold. The flow chart of the above perturbation method is shown in Fig. 1.

For a given reference medium, the calculation of w_{ijk} and I_{jk} can be considered as a forward problem. A method for the forward calculation for steady-state measurements has previously been reported [1, 2]. Recently, this method has been extended to consider time-resolved signals [6]. In the following, we discuss the solution of $\mathbf{\Delta x}$ given $\mathbf{W}$ and $\mathbf{\Delta I}$.

3 Iterative Algorithms for Solving the Perturbation Equations

The difficulties in solving the perturbation equation are three-fold. First, the dimension of the unknown $\mathbf{\Delta x}$, and hence the weight matrix $\mathbf{W}$, can be extremely large. Second, the weights for voxels far below the surface are very small, so that the matrix $\mathbf{W}$ is ill-conditioned. This makes the solution sensitive to measurement noise and numerical errors. The last, and also the most difficult to deal with, is that the problem may be underdetermined, or ill-posed. This is the case when there are fewer detector readings than voxels, i.e, $M < N$, as often will be the case when only the backscattered field is measured. The problem may still be underdetermined even when $M \geq N$, because the voxels far below the surface cannot be "seen" by any detector. Mathematically, the column vectors in $\mathbf{W}$ corresponding to the weights for deep voxels all are nearly zero and hence are correlated, which makes $\mathbf{W}$ rank-deficient. In these cases, there exist an infinite number of solutions and additional *a priori* information, e.g, of the type described in Refs. [8–10], must be incorporated to yield a correct solution.

Until now, we have concentrated on the application of iterative schemes for solving the perturbation equation. Compared to their counterparts using direct matrix inversion or pseudo-inversion, they permit progressive reconstruction and selective use of detector readings, which is very important for preliminary investigations [11]. Moreover, it is much easier to incorporate *a priori* information in iterative schemes. An

effective iterative scheme must meet at least two requirements: 1) it must converge to a correct solution, and 2) the speed of convergence cannot be too slow. In the following, we compare two iterative schemes in these regards: the CGD and POCS methods. We also present a multi-grid reconstruction algorithm which is faster and in most cases can yield better results.

3.1 Projection onto Convex Sets (POCS)

A set is *convex* if for any two elements x_1 and x_2 in the set, the linear combination $\alpha x_1 + (1-\alpha)x_2$ also belongs to the set, where $0 \leq \alpha \leq 1$. Geometrically, convex sets are the sets without holes or concave boundaries. The method of POCS is applicable in our reconstruction problem if each piece of information about the unknown medium, e.g, detector readings or other *a priori* information, confines the unknowns to a convex set, C_l, and the desired solution is in the intersection of these convex sets, i.e, $\mathbf{\Delta x} \in \cap_{l=1}^{L} C_l$. The POCS method reaches a point in the intersection by projecting a current estimate onto each set sequentially and iteratively. Letting $\mathbf{\Delta x}^{(n)}$ represent the estimate at the n-th iteration, each step in POCS can be represented by

$$\mathbf{\Delta x}^{(n+1)} = \mathcal{P}_L \circ \mathcal{P}_{L-1} \circ \cdots \mathcal{P}_1 \mathbf{\Delta x}^{(n)} \ . \tag{4}$$

Here, $\mathcal{P}_l$ represents the projection operator onto C_l such that $\mathcal{P}_l \mathbf{\Delta x}$ is the element in C_l that is closest to $\mathbf{\Delta x}$. The symbol $\circ$ denotes the sequential concatenation of two projections. The process in Eq. (4) can be relaxed by replacing $\mathcal{P}_l$ with $\mathcal{T}_l = \mathcal{I} + \lambda_l(\mathcal{P}_l - \mathcal{I})$, where λ_l are user-chosen relaxation constants, and $\mathcal{I}$ stands for the identity operation. Youla [12] has proved that, as long as the intersection of the constraint sets is not empty, iterative projections onto these sets using $0 < \lambda_l < 2$ will converge to their intersection. For a more detailed description of POCS and its applications in medical imaging, see Refs. [12, 13].

To solve the perturbation equation, each equation in (2) can be regarded as a convex set constraint described by $C_{jk} = \{\mathbf{\Delta x} \in \mathcal{R}^N : \mathbf{w}_{jk}^T \mathbf{\Delta x} = \Delta I_{jk}\}$. Here, $\mathcal{R}^N$ denotes the N-dimensional real Euclidean space. The projection onto this set can be accomplished [13] by

$$\mathcal{P}_{jk} \mathbf{\Delta x} = \mathbf{\Delta x} + \frac{\Delta I_{jk} - \mathbf{w}_{jk}^T \mathbf{\Delta x}}{\|\mathbf{w}_{jk}\|^2} \mathbf{w}_{jk} \ . \tag{5}$$

Here $\|\mathbf{w}_{jk}\|^2 = \sum_{i=1}^{N} w_{ijk}^2$. Note that the update in (5) is equivalent to the backprojection of the error in an individual reading in the algebraic reconstruction technique (ART) [14].

In addition to the measurement constraints, other *a priori* information can also be incorporated, as long as it forms convex sets. One constraint that we have used is the range constraint: $C_r = \{\mathbf{\Delta x} \in \mathcal{R}^N : \Delta x_{\min} \leq \Delta x_i \leq \Delta x_{\max}\}$. The projection operator is a simple truncation operation [13]. In our simulation, we have assumed that the real medium always has stronger absorption than the reference medium such that $\Delta x_i \geq 0$ or $\Delta x_{\min} = 0$. An appropriate $\Delta x_{\max}$ is also chosen, based on our a *priori* knowledge of the absorption properties of the test medium. The POCS method using only the measurement and range constraints is equivalent to the additive form of the weighted ART [14]. But POCS is much more general, since almost any *a priori* information that may arise in practice forms a convex set constraint and can be handled by the POCS method.

A problem with POCS is that its convergence rate can be quite slow. This is because each projection makes use of one constraint without considering others. To alleviate this problem, appropriate pre-processing should be conducted to reduce the number of unknowns as much as possible. One approach is to make further use of the positivity of Δx_i. Since ΔI_{jk} in Eq. (1) is a summation of positive numbers, if ΔI_{jk} is very small, then each term in the sum should be close to zero. This constraint is enforced by setting $\Delta x_i = 0$ if $\Delta I_{jk}/w_{ijk} \leq T$, where T is a preset threshold. When T is selected properly, this process is very effective in reducing the number of unknowns and speeding up the reconstruction process.

Another drawback of POCS is that it may fall into a "dead loop" if the constraint sets formed by the measurements fail to intersect. This is often the case in practice due to measurement noise. This problem can be circumvented by enlarging each measurement constraint set to $C_{jk} = \{\mathbf{\Delta x} \in \mathcal{R}^N : \mid \mathbf{w}_{jk}^T \mathbf{\Delta x} - \Delta I_{jk} \mid < \epsilon_{jk}\}$. The corresponding projection operator can be accordingly modified from Eq. (5). In addition, if it is known that the reconstructed image is close to the reference image, we can add another constraint set: $C_e = \{\mathbf{\Delta x} : \|\mathbf{\Delta x}\| < \epsilon\}$, where $\|\mathbf{\Delta x}\|^2 = \sum_{i=1}^{N} \Delta x_i^2$. The projection operator onto this set can be found in Ref. [13]. This projection will regularize the iterative process so that the solution is never too far from the reference image.

3.2 Least Square Solution Using Gradient Descent Methods

An alternative method for solving the perturbation equation is to minimize the following squared error:

$$E(\mathbf{\Delta x}) = \frac{1}{2}\sum_{jk}(\mathbf{w}_{jk}^T\ \mathbf{\Delta x} - \Delta I_{jk})^2 = \frac{1}{2}(\mathbf{W\Delta x} - \mathbf{\Delta I})^{\mathbf{T}}(\mathbf{W\Delta x} - \mathbf{\Delta I}). \tag{6}$$

Since E is a quadratic function of $\mathbf{\Delta x}$, the minimal point can be reached by a gradient descent method. The basic update operation in the direct descent method is described by

$$\mathbf{g} = \sum_{jk}(\mathbf{w}_{jk}^T\mathbf{\Delta x}^{(n)} - I_{jk})\mathbf{w}_{jk} = \mathbf{W}^T(\mathbf{W\Delta x}^{(n)} - \mathbf{\Delta I})\ ; \tag{7}$$

$$\mathbf{\Delta x}^{(n+1)} = \mathbf{\Delta x}^{(n)} - \alpha\mathbf{g}\ . \tag{8}$$

Here, $\mathbf{g}$ is the gradient at n-th iteration, and α is called step-size, which must be chosen appropriately to guarantee convergence. We see that the gradient vector in Eq. (7) is equivalent to the summation of the back-projections from all the readings. Hence, each update described by Eq. (8) is based on the total backprojection, similar to the simultaneous iterative reconstruction technique (SIRT) [14].

There are a variety of gradient descent methods. We have concentrated on the conjugate gradient descent (CGD) algorithm which is particularly suitable for large-scale least squares problems [5]. It modifies a current estimate in the conjugate gradient direction, which is a linear combination of the previous gradient directions. Theoretically, the CGD method can reach the optimal solution in no more than N iterations. In practice, many more iterations are required due to rounding errors. It is, nevertheless, much faster than the POCS method. In addition, it is more robust in the presence of noise, since each update is based on the total backprojection. The error in one measurement will not have as significant an effect on the final solution as that with POCS type sequential algorithms. Budinger *et al.* [15] have found that, of the many iterative techniques for image reconstruction in emission computed tomography, the best results and fastest convergence can be achieved with CGD.

One major problem with CGD is that it is reliable only for overdetermined problems. In an underdetermined setting, it simply reaches a solution that is closest to the initial point. It is very difficult to impose non-linear *a priori* constraints to force the CGD process towards the true solution. One method has been to periodically modify an intermediate solution by projecting it onto convex constraints not included in the error measure [16]. But this will slow down the convergence of the method substantially.

3.3 A Multi-Grid Reconstruction Algorithm

Facing the difficulties with POCS and CGD, a *multi-grid* progressive reconstruction scheme has been developed. It first obtains a coarse grid image in which each cell corresponds to, say, $3 \times 3 \times 3$ voxels in the original medium, and then further reconstructs the regions of interest [1] on a finer grid. The weight for a coarse cell

[1] voxels with non-zero values, in our case.

is approximated by the summation of the weights for all the voxels contained in this cell. The reconstruction at each step can be accomplished by either CGD or POCS. In most cases, the reconstruction problem at intermediate levels can be made overdetermined, and the CGD algorithm is preferable since it converges faster. Only the reconstruction at the last level needs to be accomplished by POCS if the number of remaining unknowns exceeds the number of available measurements.

Because the number of unknowns to be resolved at each level is much smaller than the total number of voxels at the final desired resolution, the multi-grid method requires much less computation than CGD or POCS. In addition, such an approach can force the iterative process to proceed in the correct direction if good solutions can be obtained at coarse resolutions. Mathematically, this is a way to prevent the iterative process from being trapped in an undesired local minimum and enforce a solution that is correct at various scales. The success of such a scheme, however, depends on the composition of the test medium and the way the coarse grids are formed. Multi-grid implementation of several iterative algorithms for image reconstruction from straight line projections has been studied [17]. A "local smoothness" property has been described as the necessary condition for the method to converge faster than the direct single grid method. This result is applicable to our problem as well.

4 Results

4.1 Media Containing Point Absorbers

To evaluate the capability of the perturbation approach to resolve absorption distributions at different depths from backscattered measurements alone, we have attempted the reconstruction of one or two closely juxtaposed point absorbers of size 1 mfp^3 buried at various depths in an isotropically scattering half-space. The absorption coefficient of the background medium is 1 %, and that of the absorber is 5 %. Only a volume of size $41 \times 41 \times 10$ mfp^3 is reconstructed, with a total of 16,810 unit-size voxels. The source and detector configurations for this experiment are illustrated in Fig. 2. The total number of detector readings is 884 within the surface of 41×41 mfp^2. Hence, the problem is severely underdetermined. The same medium without absorbers is chosen as the reference, and the weights for the reference medium were calculated using methods previously described [2]. The differences in detector readings for several absorber configurations are generated directly according to Eq. (1). This is to evaluate, in the ideal case when the perturbation model is valid, the achievable resolution of the proposed method.

Reconstruction results using various methods for a medium containing a single point absorber at depth 2–3 mfp are presented in Figs. 3(a)–(d). Fig. 3(a) illustrates one cross-section of the original medium. Fig. 3(b) and 3(c) are the reconstructed images using the CGD and POCS methods, respectively, each after 100 iterations. Only the measurement and range constraints are used with POCS. In all the figures, the gray level represents the relative increase in absorption from the reference media. The degree of darkening is in proportion to the relative increase. For display purpose, the images have been scaled to the same minimum and maximum darkness. Hence, the same gray level in separate figures may represent different absorption levels. The reconstructed images by both methods correctly reveal the existence of the absorber. But the CGD algorithm does not yield as sharp an image as the POCS method. In fact, some voxels are given values outside the correct range with the CGD method. The POCS method yields a nearly perfect reconstruction, except that the voxel below the absorber is slightly darkened.

With the multi-grid method, two levels of grids are used, the original and a coarse representation formed by grouping every $3 \times 3 \times 3$ original voxels. The CGD and POCS methods are used for the coarse and fine level reconstructions, respectively. The coarse grid solution is shown in Fig. 3(k). It is seen that it gives a good estimate of the true image. The total number of unknowns left for reconstruction in the full resolution is only 13 % of the original one. The final image obtained with POCS after 100 iterations is shown in Fig. 3(d),

which is quite similar to that by the direct POCS method. However, because of the reduction of the unknowns in the fine grid, each iteration with this method requires significantly less time. In terms of computation time, the previous POCS and CGD methods used 50 and 33 hours of computing time of a SUN Sparc workstation, while the multi-grid method required only 5 hours.

To compare the convergence behavior of the above algorithms, Fig. 4 presents their error reduction curves, where the error is as defined in Eq. (6). It is seen that the CGD algorithm has the fastest convergence rate among these methods. It also has a smaller final error, although the reconstructed image is not as close to the true image as those by the POCS and multi-grid methods. This implies that it converges to a legitimate, but wrong, solution. The convergence rates of the POCS and multi-grid methods are comparable to each other, with the latter being more uniform.

Figs. 3(e)–(j) present the results of the multi-grid method for three other point absorber configurations: a single absorber at depth of 4–5 mfp, two absorbers separated by 1 mfp at depths 2–3 and 4–5 mfp. These images are obtained with 200 iterations of POCS in the fine level. We see that the results for the media containing absorbers at 4–5 mfp are less accurate, with the darkest regions occurring at depth 3–5 mfp. Many more iterations are required to reach a better results. For example, starting with the image in Fig. 3(j), the use of additional 500 CGD iterations has produced the image in Fig. 3(l). The reason for the requirement of more iterations is that the weights for deeper voxels are much smaller than those for shallower voxels, so the iterative algorithm does not change the deeper voxels until the shallower voxels have been solved in earlier iterations.

4.2 A Medium Containing the "T" Absorber

The above results are based on calculated data. In this section, we present reconstruction results from data obtained by Monte Carlo simulations for an isotropically scattering medium containing a "T" shaped black absorber. Two orthogonal cross-sections of the actual T absorber medium are shown in Fig. 5(a). The left and right columns are the X-Z and Y-Z cross-sections of the medium, respectively. The source configuration is shown in Fig. 6; the detector position for each source is the same as shown in Fig. 2(b).

Figs. 5(b)–(d) show the reconstruction results by the CGD and multi-grid methods. They were obtained using a corresponding homogeneous medium as the reference. Note that the changes in detector readings in the presence of such a large black absorber will not follow the perturbation model accurately. Nevertheless, the reconstructed image based on this model contains a sharp darkening in the region where the "T" absorber is located. This is a very encouraging result as it suggests that even with a reference medium that is quite different from the real medium, one iteration of the perturbation method may yield useful results.

4.3 A Three-Layer Medium

To evaluate the effect of the accuracy of the reference medium on the reconstruction results, we have attempted to reconstruct a three-layer medium using a homogeneous medium as the reference. The original medium is shown in Fig. 7(a). It is 10 mfp thick, and the three layers are located from 0–3, 3–7, and 7–10 mfp, respectively. The absorption coefficient of the first and third layers is 1%, and that of the middle layer is 5%. The source–detector configuration is the same as that for the point absorber case shown in Fig. 2.

The weight functions have been calculated for both the true and reference media. These two sets of weights will be referred to as the *three-layer weights* and *half-space weights*, respectively. Two sets of readings are tested: one is calculated according to Eq. (1) using the three-layer weights; the other is obtained from Monte-Carlo simulations. In each case, the reconstruction is performed using both the three-layer and half-space weights. For simplicity, the stratified structure of the medium is assumed known. With this assumption, a perturbation equation with only 10 unknowns can be set up, each representing the absorption property of a single plane.

The weight for each plane is obtained by summing the weights for all the voxels in this plane. The POCS method is used for the solution.

The reconstructed images in various cases are shown in Figs. 7(b)–(e). Fig. 7(b) is obtained from the calculated data, using three-layer weights. The transition from the first to the second layer is accurately reconstructed, but the transition from the second to the third is blurred. When the half-space weights are used, an incorrect image resulted (Fig. 7(c)), with a darker and narrower layer appearing before the true second layer. This is reasonable since the half-space weights used in the planes within and below the second layer are larger than the true weights.

With the simulated data, when using the three-layer weights (Fig. 7(d)), the algorithm reveals correctly, with slight blurring, the three-layer structure. But the absorption level of the second layer is overestimated and its thickness is underestimated. With the half-space weights (Fig. 7(e)), the transition from the first to the second layer is further blurred, and as with the calculated data, the thickness of the second layer is underestimated. This is as expected since the perturbation model is not valid in the presence of a non-localized variation between the true and reference media. In order to obtain a more accurate reconstruction, the perturbation method should be iterated several times, as described in Sec. 2, with the reference medium and weights being updated after each step.

5 Discussion

Presently, there are mainly two classes of efforts under study for imaging dense scattering media. One class attempts to separate the unscattered or ballistic components of the injected photons from the scattered components. This may be accomplished by using ultra-fast, time-gated methods which can reject photons that take more than a preset maximum time to reach the detector [18–21], or by using holographic techniques which exclude the light not possessing the correct phase relation to a reference signal [22, 23]. These techniques have shown promise in situations where the sample thickness is not too much greater than the transport mean free pathlength.

The second class makes use of the scattered light to reconstruct an image, based on a mathematical model that relates the scattered field to the optical properties of the test medium, which is what has been considered here. A general approach has been to iteratively solve forward and inverse problems. The forward step calculates the detector readings based on the current estimates of the test medium. The inverse step modifies the previous reconstruction such that a certain error measure between the detected and calculated detector readings is minimized. This step often requires the knowledge of the gradients of the detector readings with respect to the unknown parameters, which also must be calculated in the forward step. The approach by Singer *et al* [24] and Grünbaum *et al* [25] is based on a general mathematic model derived from the discretization of the Boltzman transport equation in both the spatial and angular domains. The forward step consists of the solution of a linear equation; the inverse step is accomplished by the Levenberg–Marquardt method [5], which is equivalent to the Newton-Raphson method, when the regularization parameter is set to zero. Their approach is applicable to arbitrarily shaped objects. It also permits iterative estimation of both the absorption and scattering properties, at least in principle. However, the overwhelming amount of computation required has limited their evaluation to very small size objects. The method of Arridge *et al* [26] is derived from considering the diffusion approximation of the transport equation. The closed-form solutions of the scattered field and its gradient have been derived and used for reconstruction of cylindrical objects. Two regularized Moore-Penrose inversion methods [27] have been attempted for the inverse update, which are in principle equivalent to the Levenberg–Marquardt method.

The iterative perturbation approach described here is similar in spirit to the compensation theorem method used in EIT, which is a combination of the sensitivity theorem and the Newton Raphson method. Here, the

Newton-Raphson update is accomplished by the solution of the perturbation equation. Compared to the method by Singer *et al* [24] and Grünbaum *et al* [25], the calculation of the gradient information, that is required in the inverse step, is simplified. For isotropically scattering media with steady-state measurements, the gradient, referred to here as the weight, of the photon flux at a chosen detector for a given source with respect to the absorption property at an interior point is equal to the product of the forward and adjoint fluxes at that point due to photons injected from the source and detector, respectively [1, 2]. This result is derived using the radiation transport theory. Arridge *et al* [26] also derived this result based the diffusion approximation. They were able to evaluate analytically the weights for cylindrical objects. But for arbitrarily shaped media, numerical methods would have to be considered. Although this paper has been restricted to considering weight functions calculated for steady-state measurements in isotropic media, our methods are easily extended to anisotropic media and time-gated measurements.

The solution of the perturbation equation in the proposed method is equivalent to the Moore–Penrose pseudo-inverse [27] used by Arridge *et al.* They used regularized singular value decomposition methods to obtain the solution [26]. We resorted to iterative schemes that can incorporate *a priori* information, which is necessary to overcome the underdetermined nature of the equation. The key problems for solving the perturbation equation are how to determine and enforce appropriate *a priori* constraints. The first problem has been partially treated elsewhere [8–10]. The focus here is on the second problem. It is shown that although the CGD method converges much faster than POCS, it can yield an inaccurate answer when the problem is underdetermined. On the other hand, the POCS method, which can deal with many types of *a priori* information, progresses very slowly. The proposed multi-grid scheme computes the fine details with the help of the coarse structure and is quite effective in forcing the correct solution and reducing computation time.

Our results show that, when the difference between the initial estimate and the true medium is localized, and when using only backscattered, steady-state measurements, one step of the perturbation approach can resolve the absorption distribution at depths within 5 mfp reasonably well, at least for the examples examined here. At greater depths where the voxels have very small weights associated with all the detectors, the reconstruction is less reliable. Future work will consider the solution of the perturbation equations for time-gated measurements, and the updating of the weight functions. Preliminary results with time-gated measurements are presented in [6].

Recently, Schlereth *et al* [28, 29] have formulated the recovery problem as a learning problem in a neural net structure, taken suggestions from Singer *et al* [24]. The method iteratively updates a current estimate (the node properties) until the values of the photon fluxes (the output of the net) match those detected (the training vector). This method appears to offer greater flexibility in modeling the forward problem, and yields accurate and numerically stable results when provided with an initial estimate of the structure of the test medium.

6 References

[1] R. L. Barbour, H. Graber, R. Aronson and J. Lubowsky, "Model for 3-d optical imaging of tissue," in *Proc. 10th Annual Int. Geoscience and Remote Sensing Symposium*, vol. II, pp. 1395–1399, 1990.

[2] R. L. Barbour, H. L. Graber, R. Aronson and J. Lubowsky, "Imaging of subsurface regions of random media by remote sensing," in *Proc. Time-Resolved Spectroscopy and Imaging of Tissues*, vol. SPIE–1431, (Los Angeles), pp. 192–203, Jan. 1991.

[3] J. R. Lamarsh, *Nuclear Reactor Theory.* Addison–Wesley Publishing Co., Reading, MA, 1966.

[4] J. G. Webster, ed., *Electrical Impedance Tomography.* Bristol, England: Adam Hilger, 1990.

[5] P. E. Gill, W. Murray and M. H. Wright, *Practical Optimization.* Academic Press, 1981.

[6] R. L. Barbour, H. L. Graber, R. Aronson and J. Lubowsky, "Imaging of diffusing media by a progressive iterative backprojection method using time-domain data," Accompanying paper in these proceedings.

[7] A. Ishimaru, *Wave Propagation and Scattering in Random Media.* Academic Press, 1978.

[8] R. L. Barbour, H. L. Graber, R. Aronson and J. Lubowsky, "Determination of macroscopic optical properties of random media by remote sensing," in *Proc. Time-Resolved Spectroscopy and Imaging of Tissues*, vol. SPIE–1431, (Los Angeles), pp. 52–62, Jan. 1991.

[9] R. Aronson, "Getting under the skin with diffusion theory," in *Proc. 12-th Int. Conf. Transport Theory*, (Albuquerque), Aug. 1991. In press.

[10] H. L. Graber, R. L. Barbour, J. Lubowsky, R. Aronson, B. B. Das, K. M. Yoo and R. R. Alfano, "Evaluation of steady state, time-, and frequency-domain data for the problem of optical diffusion tomography," Accompanying paper in these proceedings.

[11] Y. Censor, "Finite series-expansion reconstruction methods," *Proceedings of IEEE*, vol. 71, pp. 409–419, 1983.

[12] D. C. Youla and H. Webb, "Image restoration by the method of convex projections onto convex sets – Part I," *IEEE Trans. Med. Imaging*, vol. MI-1, pp. 81–94, Oct. 1982.

[13] P. Oskoui-Fard and H. Stark, "Tomographic image reconstruction using the theory of convex projections," *IEEE Trans. Med. Imaging*, vol. MI-7, pp. 45–58, Mar. 1988.

[14] A. C. Kak and M. Slaney, *Principles of Computerized Tomographic Imaging.* IEEE Press, 1988.

[15] T. F. Budinger, G. T. Gullberg and R. H. Huesman, "Emission computed tomography," in *Image Reconstruction From Projections – Implementation and Applications* (G. T. Herman, ed.), Spring-Verlag, 1979.

[16] A. K. Katsaggelos and S. N. Efstratiadis, "A class of iterative signal restoration algorithms," *IEEE Trans. Acoust., Speech, Signal Processing*, vol. ASSP-38, pp. 778–786, May. 1990.

[17] T. S. Pan and A. E. Yagle, "Numerical study of multigrid implementation of some iterative reconstruction algorithms," *IEEE Trans. Medical Imaging*, vol. MI-10, pp. 572–588, Dec. 1991.

[18] R. R. Alfano, P. P. Ho and K. M. Yoo, "Photons for prompt tumor detection," *Physics World*, vol. 5, pp. 37–40, 1992.

[19] L. Wang, P. P. Ho, C. Liu, G. Zhang and R. R. Alfano, "Ballistic 2-d imaging through scattering walls using an ultrafast optical Kerr gate," *Science*, vol. 253, pp. 769–771, 1991.

[20] G. Hebden and R. A. Kruger, "A time-of-flight breast imaging system: spatial resolution performance," in *Proc. Time-Resolved Spectroscopy and Imaging of Tissues*, vol. SPIE–1431, pp. 225–231, 1991.

[21] B. Chance *et al.*, "Comparison of time-resolved and unresolved measurements of deoxyhemoglobin in brain," *Proc. Nat. Acad. Sci.*, vol. 85, pp. 4971–4975, 1988.

[22] K. G. Spears, T. Serafin, N. H. Abramson, X. Zhu and H. Bjelkhagen, "Chrono-coherent imaging for medicine," *IEEE Trans. Biomedical Eng.*, vol. 36, pp. 1210–1221, 1989.

[23] A. Rebane and J. Feinberg, "Time-resolved holograph," *Nature*, vol. 351, pp. 378–380, 1991.

[24] J. R. Singer, F. A. Grünbaum, P. Kohn and J.P. Zubelli, "Image reconstruction of the interior of bodies that diffuse radiation," *Science*, vol. 248, pp. 990–993, 1990.

[25] F. A. Grünbaum, P. Kohn, G. A. Latham, J. R. Singer and J.P. Zubelli, "Diffuse tomography," in *Proc. Time-Resolved Spectroscopy and Imaging of Tissues*, vol. SPIE–1431, pp. 232–238, Jan., 1991.

[26] S. R. Arridge, P. van der Zee, M. Cope and D. T. Delpy, "Reconstruction methods for infra-red absorption imaging," *ibid* , pp. 204–215, 1991.

[27] A. Albert, *Regression and the Moore-Penrose Pseudoinverse.* Academic Press, NY, 1972.

[28] F. H. Schlereth, J. M. Fossaceca, A. D. Keckler and R. L. Barbour, "Multicomputer based neural networks for imaging in random media," in *Proc. IEEE Nuclear Science Symposium*, Nov. 1991. In press.

[29] F. H. Schlereth, J. M. Fossaceca, A. D. Keckler and R. L. Barbour, "Imaging of diffusing media with a neural net formulation: A problem in large scale computation," Accompanying paper in these proceedings.

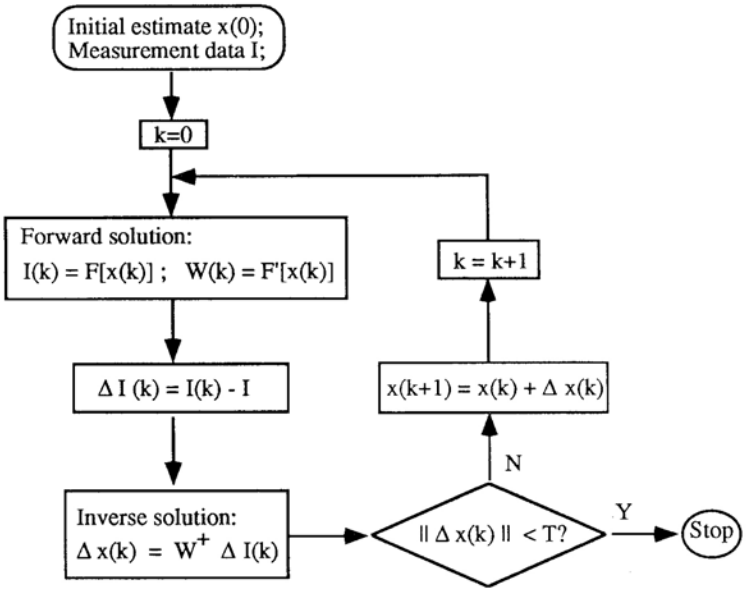

Figure 1: Iterative perturbation approach. F represents the function relating x and I. F' represents the gradient. W^+represents the generalized inverse solution of the perturbation equation.

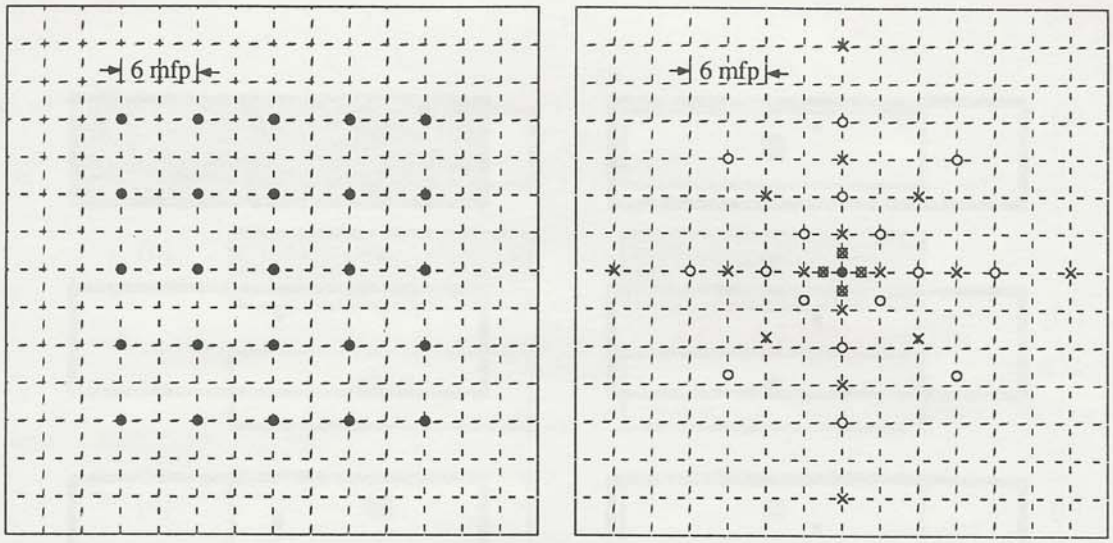

Figure 2: (a) Source locations for the point absorber and the three-layer simulations; (b) Position and orientation of detectors about each source: "o" and "×" indicate positions at which the detector was inclined 10 ° and 80 ° from the normal, respectively. "▣" indicate positions in which measurements were made in both orientations. In every measurement, the azimuthal angle of the detector was chosen such that the source and detector axes intersected at a point below the surface (z>0). Each detector received photons within a cone extending 10 ° from the centered axis, for an acceptance solid angle of ~.095 sr. See Graber *et al* [10] for more extensive description of Monte--Carlo simulations.

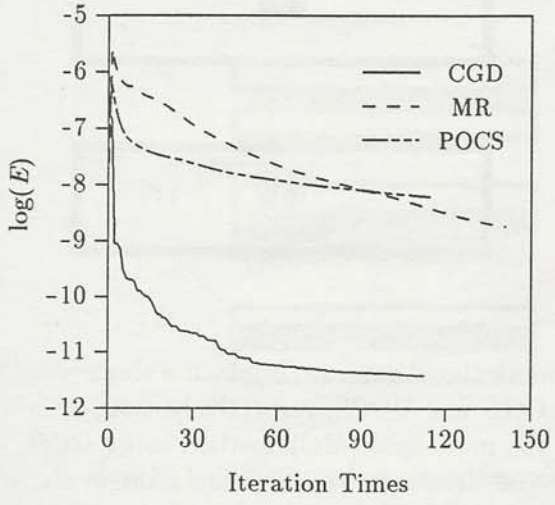

Figure 4: Convergence behaviors of CGD, POCS, and multi-grid methods for the medium shown in Fig. 3(a).

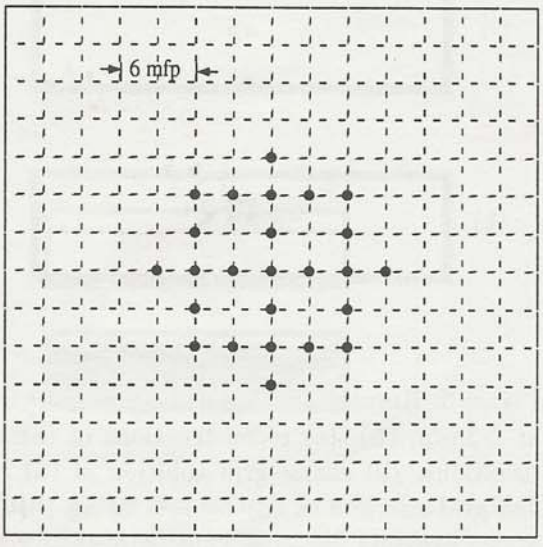

Figure 6: Source locations for the T absorber simulation. The detector position for each source is the same as in Fig. 2(b).

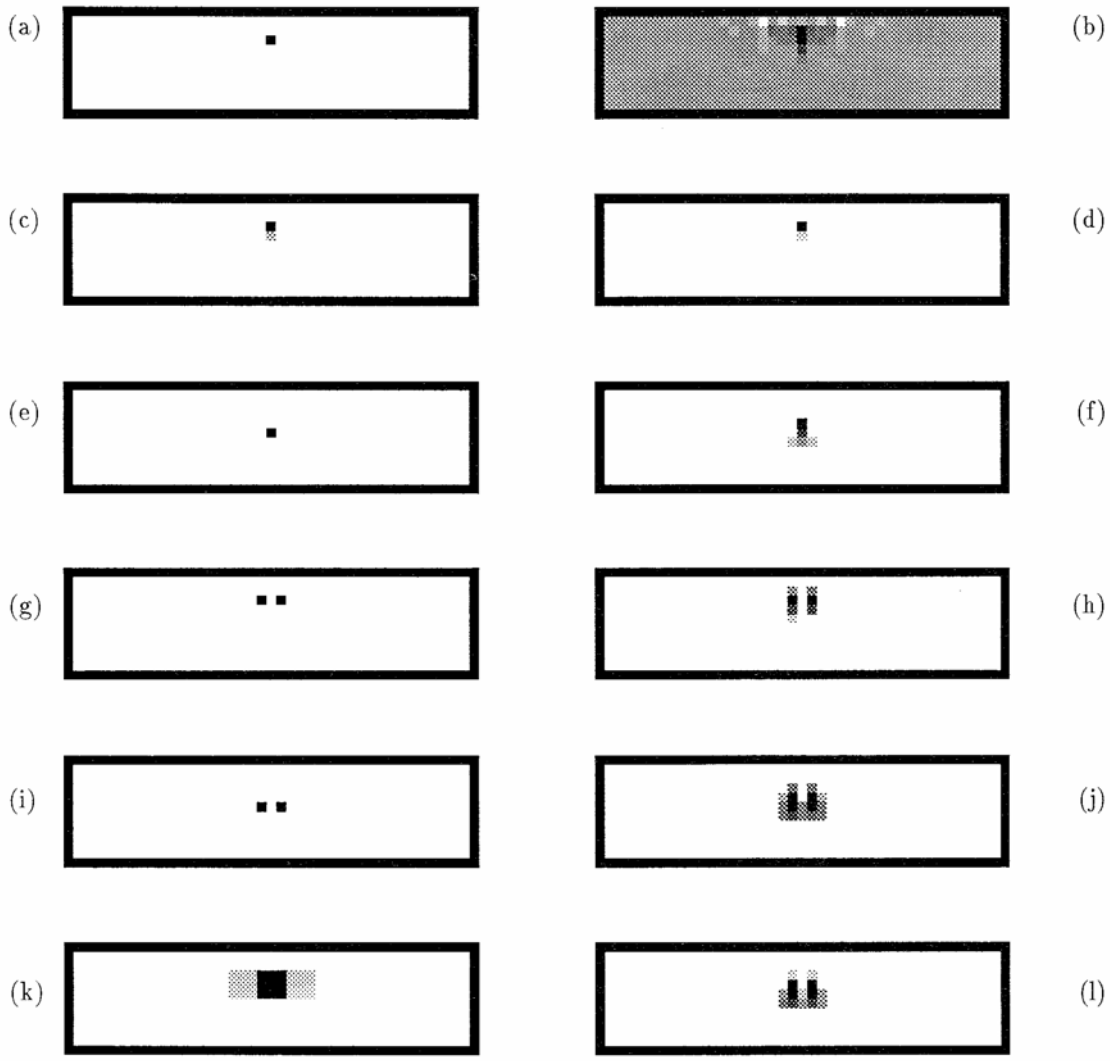

Figure 3: Results for point absorber media from calculated data: (a) original: a single absorber at 2-3mfp; (b), (c) reconstructions of (a) by CGD and POCS, respectively, both after 100 iterations; (k) coarse-grid solution of (a) by the multi-grid (MG) method using CGD; (d) fine-grid solution of (a) by MG using POCS, 100 iterations; (e) original: a single absorber at 4-5 mfp; (f) fine-grid solution of (e) by MG using POCS, 200 iterations; (g) original: two absorbers 1 mfp apart at depth 2-3 mfp; (h) fine-grid solution of (g) by MG using POCS, 200 iterations; (i) original: two absorbers 1 mfp apart at depth 4-5 mfp; (j) fine-grid solution of (i) by MG using POCS, 200 iterations; (l) fine-grid solution of (i) by MG with additional 500 CGD iterations starting from (j).

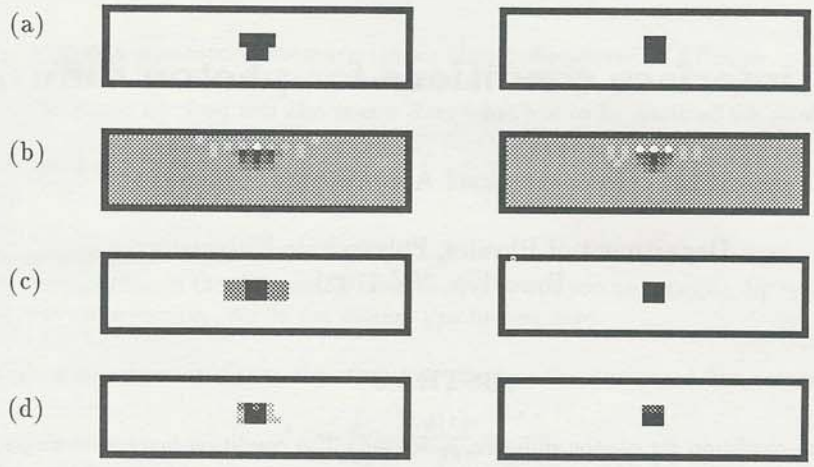

Figure 5: Results for the "T" absorber medium using Monte-Carlo data. Left column: X-Z cross-section, right column: Y-Z cross-section. Within each column: (a) original medium, (b) reconstruction by CGD, 200 iterations; (c) coarse-grid solution by MG using CGD; and (d) fine-grid solution by MG using POCS, 200 iterations.

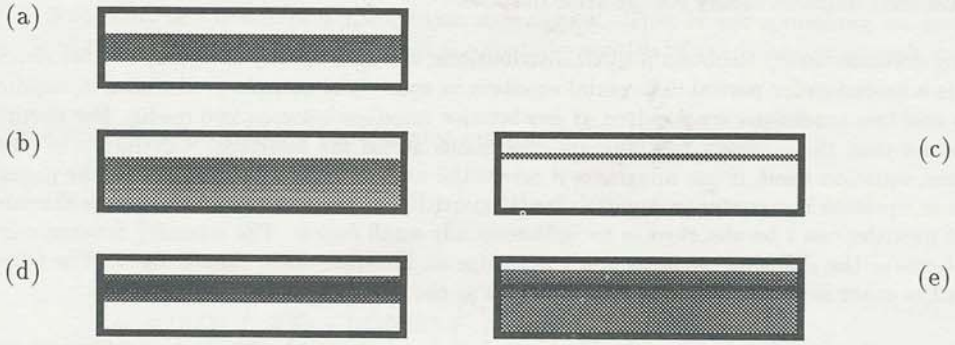

Figure 7: Results for the three layer medium assuming planar structure is known: (a) original medium; (b–c) reconstructions from calculated data using the three-layer (b) and half-space (c) weights; (d–e) reconstructions from Monte-Carlo data using three-layer (d) and half-space (e) weights.